

1 **Title:** Seasonal response of air-water CO₂ exchange along the land-ocean aquatic continuum
2 of the Northeast American coast

3 **Authors:** Goulven G. Laruelle^{1,2}, Ronny Lauerwald^{1,3}, Julie Rotschi^{1,4}, Peter A. Raymond⁵,
4 Jens Hartmann⁶, Pierre Regnier¹

Deleted:

Deleted:

Deleted:

5
6 ¹ Dept. of Earth & Environmental Sciences, CP 160/02, Université Libre de Bruxelles, 1050
7 Bruxelles, Belgium

8 ² Department of Earth Sciences - Geochemistry, Faculty of Geosciences, Utrecht University,
9 3508 TA Utrecht, Netherlands

10 ³ Institut Pierre-Simon Laplace, CNRS – FR636, 78280 Guyancourt cedex, France

11 ⁴ Department of Bioscience - Center for Geomicrobiology, Aarhus University, 8000 Aarhus
12 C, Denmark

13 ⁵ Yale School of Forestry and Environmental Studies, New Haven, Connecticut 06511, USA,

14 ⁶ Institute for Geology, KlimaCampus, Universität Hamburg, Bundesstrasse 55, 20146
15 Hamburg, Germany

16

17 Corresponding author: Goulven G. Laruelle

18 (tel: +32 2 650 42 68, goulven.gildas.laruelle@ulb.ac.be)

19

20

24 **Abstract:**

25 This regional study quantifies the CO₂ exchange at the air-water interface along the land-
26 ocean aquatic continuum (LOAC) of the Northeast American coast, from streams to the shelf
27 break. Our analysis explicitly accounts for spatial and seasonal variability in the CO₂ fluxes.
28 The yearly integrated budget reveals the gradual change in the intensity of the CO₂ exchange
29 at the air-water interface, from a strong source towards the atmosphere in streams and rivers
30 (3.0 ± 0.5 TgC yr⁻¹) and estuaries (0.8 ± 0.5 TgC yr⁻¹) to a net sink in continental shelf waters
31 (-1.7 ± 0.3 TgC yr⁻¹). Significant differences in flux intensity and their seasonal response to
32 climate variations is observed between the North and South sections of the study area, both in
33 rivers and coastal waters. Ice cover, snow melt and intensity of the carbon removal efficiency
34 through the estuarine filter are identified as important control factors of the observed spatio-
35 temporal variability in CO₂ exchange along the LOAC.

36

37

38 1. Introduction

39 Over the past decade, several syntheses have highlighted the significant contribution
40 of the Land-Ocean Aquatic Continuum (LOAC) to the global atmospheric CO₂ budget (Cole
41 et al., 2007; Battin et al., 2009; Mackenzie et al., 2012; Bauer et al., 2013; Ciais et al., 2013;
42 Raymond et al., 2013; Regnier et al., 2013). In a recent review, Regnier et al. (2013) proposed
43 that inland waters (streams, rivers and lakes) and estuaries outgas 1.1 and 0.25 PgC yr⁻¹,
44 respectively, while continental shelf seas take up 0.2 PgC yr⁻¹. However, CO₂ data are too
45 sparse and unevenly distributed to provide global coverage and large uncertainties remain
46 associated to these estimates. The inland water outgassing could for instance reach 2.1 PgC
47 yr⁻¹ with 86% coming from streams and rivers (Raymond et al., 2013), a value which is about
48 twice that reported in Regnier et al. (2013) and in the 5th assessment report of the IPCC (Ciais
49 et al., 2013). The most recent global budgets for the estuarine CO₂ source and the continental
50 shelf CO₂ sink also reveal significant discrepancies, both falling within the 0.15-0.4 PgC yr⁻¹
51 range (Laruelle et al., 2010; Cai, 2011; Bauer et al., 2013; Dai et al., 2013; Laruelle et al.,
52 2013). None of these estimates, however, fully resolves the seasonality in CO₂ fluxes because
53 temporal coverage of the global data is insufficient. Complex seasonal dynamics of CO₂
54 exchanges between the atmosphere and individual components of the LOAC have been
55 reported in previous studies which have highlighted the potential importance of the intra-
56 annual variability for local and regional CO₂ budgets (e.g. Kempe 1982; Frankignoulle, et al.,
57 1998; Jones and Mulholland, 1998; Degrandpré et al., 2002; Thomas and Schneider, 1999;
58 Wallin et al., 2011; Regnier et al., 2013; Rawlins et al., 2014). Here, we extend the analysis to
59 the sub-continental scale, and present the spatial and seasonal variability of CO₂ fluxes at the
60 air-water interface (FCO₂) for the entire Northeast American LOAC, from streams to the shelf
61 break. This region of unprecedented data coverage allows us producing, for the first time,
62 empirically-derived monthly maps of CO₂ exchange at 0.25° resolution. Our results allow

63 investigating the seasonal CO₂ dynamics across the inter-connected systems of the LOAC and
64 elucidating their response to contrasting intra-annual changes in climate conditions.

65

66 2. Methods

67 Our study area is located along the Atlantic coast of the Northern US and Southern
68 Canada and extends from the Albemarle Sound in the South to the Eastern tip of Nova Scotia
69 in the North. It corresponds to COSCAT 827 (for Coastal Segmentation and related
70 CATCHments) in the global coastal segmentation defined for continental land masses by
71 Meybeck et al. (2006) and extrapolated to continental shelf waters by Laruelle et al. (2013).
72 COSCATs are homogenous geographical units that divide the global coastline into
73 homogeneous segments according to lithological, morphological, climatic and hydrological
74 properties. The area corresponding to COSCAT 827 comprises 447 10³ km² of watersheds
75 and 357 10³ km² of coastal waters, amongst which 15 10³ km² of estuaries. It is one of the
76 best monitored regions in the world with several regularly surveyed rivers (Hudson,
77 Susquehanna, York, Connecticut) and some of the most extensively studied coastal waters
78 (Degrandpré et al., 2002; Chavez et al., 2007; Fennel et al., 2008; Fennel and Wilkin, 2009;
79 Previdi et al., 2009; Fennel, 2010; Shadwick et al., 2010; 2011; Signorini et al., 2013). For the
80 purpose of this study, the area was divided in a North and a South section (Fig. 1). The
81 boundary is set on land, to delineate the regions subject to seasonal ice freeze and snowfalls
82 from those that are not (Armstrong and Brodzik, 2001). This delineation attributes 96% of the
83 estuarine surface area to the South section due, for the most part, to the contribution of
84 Chesapeake Bay which accounts for about two thirds of the estuarine area. The delineation
85 extends further into the coastal waters in such a way that the Scotian Shelf and the Gulf of
86 Maine correspond to the North section and the Mid-Atlantic Bight and Georges Bank to the

Deleted: s

South section. The riverine data are calculated from pH and alkalinity measurements extracted from the GLObal RIVER CHemistry Database (GLORICH, previously used in Lauerwald et al., 2013) while continental shelf values are calculated from the Surface Ocean CO₂ Atlas (SOCAT v2.0) database which contains quality controlled direct pCO₂ measurements (<http://www.socat.info/>, Bakker et al., 2014).

2.1. Rivers

CO₂ evasion from rivers (FCO₂) was calculated monthly per 15s grid cell (resolution of the hydrological routing scheme Hydrosheds 15s, Lehner et al., 2008) from estimates of the effective stream/river surface area A_{eff} [m²], gas exchange velocity k [m d⁻¹], and water-atmosphere CO₂ concentration gradient $\Delta[\text{CO}_2]$ [μmol l⁻¹]:

$$FCO_2 = A_{\text{eff}} \times k \times \Delta[\text{CO}_2] \quad (\text{Eq. 1})$$

The calculation of A_{eff} first requires estimation of the total stream/river surface area, A. The latter was calculated from the linear stream network derived from the Hydrosheds 15s routing scheme using a minimum threshold on the catchment area of 10 km² and estimates of stream width derived from the annual mean discharge Q_{ann} using the equations of Raymond et al. (2012, 2013) (Eqs. 2,3). A values were not calculated for each individual month, as the discharge-stream width relations only hold true for Q_{ann} (Raymond et al., 2013). Q_{ann} was obtained using Hydrosheds 15s to route the gridded data of average annual runoff from the UNH/GRDC composites (Fekete et al., 2002).

$$\ln(B \text{ [m]}) = 2.56 + 0.423 \cdot \ln(Q_{\text{ann}} \text{ [m}^3\text{s}^{-1}\text{]}) \quad (\text{Eq 2, after Raymond et al., 2012})$$

$$\ln(B \text{ [m]}) = 1.86 + 0.51 \cdot \ln(Q_{\text{ann}} \text{ [m}^3\text{s}^{-1}\text{]}) \quad (\text{Eq. 3, after Raymond et al., 2013})$$

with

B stream width [m]

111 Q_{ann} annual average discharge [$\text{m}^3 \text{s}^{-1}$]

112 For each 15s raster cell covered by lake and reservoir areas as represented in the
113 global lake and wetland data base of Lehner and Döll (2004), A was set to 0 km^2 . A_{eff} was
114 then derived from A to account for seasonal stream drying and ice cover inhibiting FCO_2 .
115 Seasonal stream drying was assumed for each 15s cell and month when the monthly average
116 discharge Q_{month} is 0 $\text{m}^3 \text{s}^{-1}$. Values of Q_{month} were calculated similarly to that of Q_{ann} using the
117 gridded data of average monthly runoff from the UNH/GRDC composites (Fekete et al.,
118 2002). Ice cover was assumed for each 15s cell and month when the mean air temperature
119 (T_{air}), derived from the worldclim data set of Hijmans et al. (2005), is below -4.8°C
120 (Lauerwald et al., under revision). In case of ice cover and/or stream drying, A_{eff} is set to 0
121 m^2 . Otherwise A_{eff} equals A.

122 Values of k were first calculated as standardized values for CO_2 at a water temperature
123 (T_{water}) of 20°C (k_{600}), from stream channel slope CS and estimates of flowing velocity V (Eq
124 4). Using the Strahler order (Strahler, 1952) to perform the segmentation of the stream
125 network, CS was calculated for each segment by dividing the change in its altitude by its
126 length. Information on altitude was derived from the Hydrosheds elevation model. V was
127 calculated from Q_{ann} based on the equations of Raymond et al. (2012, 2013) (Eqs. 5, 6).
128 Similarly to the stream width, the V-Q relations only hold true for Q_{ann} (Raymond et al.,
129 2013), and this is why only annually average values for V and k_{600} could be calculated. The k
130 value for each month was calculated from k_{600} an estimate of the average monthly water
131 temperature T_{water} (Lauerwald et al., under revision; Raymond et al., 2012).

132 $k_{600} [\text{m d}^{-1}] = V [\text{m s}^{-1}] \cdot CS [1] \cdot 2841 + 2.02$ (Eq. 4, after Raymond et al., 2012)

133 $\ln(V [\text{m s}^{-1}]) = -1.64 + 0.285 \cdot \ln(Q_{ann} [\text{m}^3 \text{s}^{-1}])$ (Eq. 5, after Raymond et al., 2012)

134 $\ln(V [\text{m s}^{-1}]) = -1.06 + 0.12 \cdot \ln(Q_{ann} [\text{m}^3 \text{s}^{-1}])$ (Eq. 6, after Raymond et al., 2013)

135 with

136 k_{600} Standardized gas exchange velocity for CO_2 at 20°C water temperature [m d^{-1}]

137 Q_{ann} annual average discharge [$\text{m}^3 \text{s}^{-1}$]

138 V stream flow velocity [m s^{-1}]

139 CS channel slope [dimensionless]

140

141 Values of $\Delta(\text{CO}_2)$ were derived from monitoring data with calculated $\text{pCO}_{2\text{river}}$ (12,300
142 water samples, from 161 locations, Lauerwald et al., 2013), an assumed $\text{pCO}_{2\text{atmosphere}}$ of 390
143 μatm . Lauerwald et al. (2013) calculated $\text{pCO}_{2\text{river}}$ values from pH, alkalinity, water
144 temperature, and, where available, major ion concentrations, using the hydrochemical
145 modelling software PhreeqC v2 (Parkhurst & Appelo, 1999). The pCO_2 values were
146 converted into concentrations, $[\text{CO}_2]$, using Henry's constant (Henry, 1803) for each sample
147 at its observed temperature T_{water} using the equation of Telmer and Veizer (1999). In order to
148 minimize the influence of extreme values, the results were aggregated to median values per
149 sampling location and month for which at least three values were available. These median
150 values per sampling location and month were then used to calculate maps of $\Delta[\text{CO}_2]$ at a 15s
151 resolution. To this end, an inverse distance weighted interpolation was applied. This method
152 allows predicting a value for each grid cell from observed values at the four closest sampling
153 locations, using the inverse of the squared distance between the position on the grid and each
154 sampling locations as weighting factors. To account for downstream decreases in $\text{pCO}_{2\text{river}}$,
155 which are often reported in the literature (Finlay, 2003; Teodoru et al., 2009; Butman and
156 Raymond, 2011), the interpolation was applied separately to three different classes of streams
157 and rivers defined by Q_{ann} , for which sufficiently large subsets of sampling locations could be
158 retained: 1) $Q_{\text{ann}} < 10 \text{ m}^3 \text{s}^{-1}$ ($n = 76$), 2) $10 \text{ m}^3 \text{s}^{-1} \leq Q_{\text{ann}} < 100 \text{ m}^3 \text{s}^{-1}$ ($n = 47$), and 3) $Q_{\text{ann}} \geq 100 \text{ m}^3 \text{s}^{-1}$
159 ($n = 38$). The three maps of $\Delta[\text{CO}_2]$ per month were then recombined according to the

spatial distribution of Q_{ann} values. The FCO_2 values were first calculated using equation (1) at the high spatial resolution of 15s for each month. The results were then aggregated to a 0.25° resolution and three-month period and reported as area specific values referring to the total surface area of the grid cell. At the outer boundaries, only the proportions of the cell covered by our study area are taken into account. The difference between the FCO_2 s calculated using the equations of Raymond et al. (2012) and Raymond et al. (2013) was used as an estimate of the uncertainty of the mean yearly FCO_2 . This method is consistent with the approach of Raymond et al. (2013), which used two distinct sets of equations for k and A to estimate the uncertainty in these parameters and their combined effect on the estimated FCO_2 .

2.2. Estuaries

The yearly averaged CO_2 exchange at the air-water interface was obtained from local estimations of emission rates in seven estuaries located within the study area (see Table 1). The limited number of observation does not allow resolving the seasonality in CO_2 emissions. The yearly-average local CO_2 emission rates range from $1.1 \text{ molC m}^{-2} \text{ yr}^{-1}$ in the Parker River to $9.6 \text{ molC m}^{-2} \text{ yr}^{-1}$ in the Hudson River estuary, for a mean value of $4.2 \text{ molC m}^{-2} \text{ yr}^{-1}$ for the seven systems. This value was then multiplied by the estuarine surface areas extracted from the SRTM water body data set (NASA/NGA, 2003), to estimate the bulk outgassing for the North and South sections of COSCAT 827. It should be noted that the methods used to estimates the CO_2 emission rates differ from one study to the other (i.e. different relationships relating wind speed to the gas transfer coefficient). However, in the absence of consistent and substantial estuarine pCO_2 database for the region, we believe that our method is the only one which allows deriving a regional data driven estimate for the CO_2 outgassing from estuaries. Similar approaches have been used in the past to produce global estuarine CO_2 budgets

(Borges et al., 2005; Laruelle et al., 2010; Cai, 2011; Chen et al., 2013; Laruelle et al., 2013). Similar approaches have been used in the past to produce global estuarine CO₂ budgets (Borges et al., 2005; Laruelle et al., 2010; Cai, 2011; Chen et al., 2013; Laruelle et al., 2013). The standard deviation calculated for the emission rates of all local studies was used as an estimate of the uncertainty of the regional estuarine FCO₂.

2.3. Continental shelf waters

Monthly CO₂ exchange rates at the air-water interface were calculated in continental shelf waters using 274,291 pCO₂ measurements extracted from the SOCAT 2.0 database (Baker et al., 2014). For each measurement, an instantaneous local CO₂ exchange rate with the atmosphere was calculated using Wanninkhof's equation (Wanninkhof, 1992) which is a function of a transfer coefficient (k), dependent on the square of the wind speed above sea surface, the apparent solubility of CO₂ in water (K'_0) [moles m⁻³ atm⁻¹], which depends on surface water temperature and salinity, and the gradient of pCO₂ at the air-water interface (ΔpCO_2) [μ atm].

$$FCO_2 = A_s \times k \times K'_0 \times \Delta pCO_2 \quad (\text{Eq. 2})$$

The parameterization used for k is that of Wanninkhof et al. (2013) and all the data necessary for the calculations are available in SOCAT 2.0 except for wind speed, which was extracted from the CCMP database (Altas et al., 2011). The resulting CO₂ exchange rates were then averaged per month for each 0.25° cell in which data were available. Average monthly CO₂ exchange rates were calculated for the North and South sections using the water surface area and weighted rate for each cell and those averages were then extrapolated to the entire surface area A_s of the corresponding section to produce FCO₂. In effect, this corresponds to applying the average exchange rate of the section to the cells devoid of data.

To refine further the budget, a similar procedure was also applied to 5 depth segments (S1 to S5) corresponding to 0-20m, 20-50m, 50-80m, 80-120m and 120-150m, respectively, and their respective surfaces areas were extracted from a high resolution bathymetric files (Laruelle et al., 2013). The choice of slightly different methodologies for FCO₂ calculations in rivers and continental shelf waters stems from the better data coverage in the continental shelf, which allows capturing the spatial heterogeneity within the region without using interpolation techniques. The standard deviation calculated for all the grid cells of the integration domain was used as uncertainty of the yearly estimates of FCO₂. A more detailed description of the methodology applied to continental shelf waters at the global scale is available in Laruelle et al. (2014).

3. Results and Discussion

Figure 2 shows the spatial distribution of FCO₂ along the LOAC integrated per season. Throughout the year, river waters are a strong source of CO₂ for the atmosphere. Significant differences in the intensity of the CO₂ exchange at the air-water interface can nevertheless be observed between the North and South sections, both in time and space. During winter, there is nearly no CO₂ evasion from rivers in the North due to ice coverage and stream drying. Over the same period, the CO₂ emissions from the South section range from 0 to 5 gC m⁻² season⁻¹. During spring, the pattern is reversed and northern rivers exhibit higher outgassing rates than in the South with maximum emissions rates of >10 gC m⁻² season⁻¹. This trend is maintained throughout summer while during fall, the entire COSCAT displays similar emission rates without clear latitudinal signal.

Continental shelf waters display a very different spatial and seasonal pattern than that of rivers. During winter, the North section is predominantly a mild CO₂ sink, with rates

comprised between +2 and -5 gC m⁻² season⁻¹, which intensifies significantly in the South section (-2 to >-10 gC m⁻² season⁻¹). During spring, an opposite trend is observed with a quasi-neutral CO₂ uptake in the South and a strong uptake in the North, especially on the Scotian Shelf. The entire COSCAT becomes a net CO₂ source in summer with emission rates as high as 5 gC m⁻² season⁻¹ in the Mid-Atlantic Bight. During fall, the Gulf of Maine and Georges Bank remain CO₂ sources while the Scotian Shelf and the Mid-Atlantic Bight become again regions of net CO₂ uptake.

Deleted: s

The monthly integrated FCO₂ for the North and South sections provides further evidence of the contrasting seasonal dynamics for the two areas (Fig. 3a and 3b). In the North section, CO₂ evasion from rivers is almost zero in January and February, rises to a maximum value of 0.26 ± 0.05 TgC month⁻¹ in May, and then progressively decreases until the end of the year. These low winter values are explained by the ice cover inhibiting the gas exchange with the atmosphere. The steep increase and FCO₂ maximum in spring can be related to the flushing of water from the thawing top-soils, which is rich in DOC and CO₂. Additionally, the temperature rise also induces an increase in respiration rates within the water streams (Jones and Mulholland, 1998; Striegl et al., 2007). Rivers and the continental shelf in the North section present synchronized opposite behaviors from winter through spring. In the shelf, a mild carbon uptake takes place in January and February (-0.04 ± 0.25 TgC month⁻¹) followed by a maximum uptake rate in April (-0.50 ± 0.20 TgC month⁻¹). This CO₂ uptake in spring has been attributed to photosynthesis associated to the seasonal phytoplankton bloom (Shadwick et al., 2010). Continental shelf waters behave quasi neutral during summer ($<0.05 \pm 0.09$ TgC month⁻¹) and emit CO₂ at a high rate in November and December ($>0.15 \pm 0.21$ TgC month⁻¹). Overall, the rivers of the North section emit 1.31 ± 0.24 TgC yr⁻¹ while the continental shelf waters take up 0.47 ± 0.17 TgC yr⁻¹. The very limited estuarine surface area ($0.5 \cdot 10^3$ km²) only yields an annual outgasing of 0.03 ± 0.02 TgC yr⁻¹. The shelf sink calculated for the

region differs from that of Shadwick et al. (2011) which reports a source for the Scotian Shelves, in contrast to the current estimate. Our seasonally resolved budget is however in line with the -0.6 TgC yr^{-1} sink calculated by Signorini et al. (2013) using a 8 years dataset as well as with the simulations of Fennel and Wilkin (2009) which also predict sinks of -0.7 TgC yr^{-1} and -0.6 TgC yr^{-1} for 2004 and 2005, respectively. No similar analysis was so far performed for inland waters.

In the South section of the COSCAT, the warmer winter temperature leads to the absence of ice cover (Armstrong and Brodzik, 2001). Our calculations predict that the riverine surface area remains stable over time, favoring a relatively constant outgassing comprised between 0.1 and $0.2 \text{ TgC month}^{-1}$ throughout the year, adding up to a yearly source of $1.69 \pm 0.31 \text{ TgC yr}^{-1}$. Estuaries emit $0.73 \pm 0.45 \text{ TgC yr}^{-1}$, because of their comparatively large surface area ($14.5 \cdot 10^3 \text{ km}^2$), about one order of magnitude larger than that of rivers ($1.2 \cdot 10^3 \text{ km}^2$, Table 2). It should be noted that our estimate of the estuarine outgassing is derived from a limited number of local studies, none of which were performed in the two largest systems of COSCAT827, that are, the Chesapeake and Delaware Bays ($>80 \%$ of the total estuarine surface area in COSCAT827). These estuaries are highly eutrophic (Cai, 2011), which suggests that they might be characterized by lower $p\text{CO}_2$ values and subsequent CO_2 exchange than the other systems in the region. On the other hand our regional outgassing of $50 \text{ gC m}^{-2} \text{ yr}^{-1}$ is already well below the global average of $218 \text{ gC m}^{-2} \text{ yr}^{-1}$ calculated using the same approach by Laruelle et al. (2013) for tidal estuaries. The continental shelf CO_2 sink is strongest in January ($-0.47 \pm 0.30 \text{ TgC month}^{-1}$) and decreases until June, when a period of moderate CO_2 emission begins (max of $0.13 \pm 0.08 \text{ TgC month}^{-1}$ in August) and lasts until October. Finally, November and December are characterized by mild CO_2 sinks. Such seasonal signal, following that of water temperature, is consistent with the hypothesis of a

CO₂ exchange in the South section regulated by variations in gas solubility, as suggested by Degrandpré et al. (2002) for the Mid-Atlantic Bight.

The analysis of the intensity of the river CO₂ outgassing reveals that the smallest streams ($Q < 1 \text{ m}^3 \text{ s}^{-1}$, Q1 in table 2) display the highest emission rates per unit surface area, with values ranging from $1961 \text{ gC m}^{-2} \text{ yr}^{-1}$ in the South section to $2893 \text{ gC m}^{-2} \text{ yr}^{-1}$ in the North section. These values gradually decrease with increasing river discharge to $729 \text{ gC m}^{-2} \text{ yr}^{-1}$ in the South section and $891 \text{ gC m}^{-2} \text{ yr}^{-1}$ in the North section for $Q > 100 \text{ m}^3 \text{ s}^{-1}$ (Q4, table 2). The emission rates for this latter class of rivers are consistent with the median emission rate of $720 \text{ gC m}^{-2} \text{ yr}^{-1}$ proposed by Aufdenkampe et al. (2011) for temperate rivers with widths larger than 60-100m. Aufdenkampe et al. (2011) also report a median emission rates of $2600 \text{ gC m}^{-2} \text{ yr}^{-1}$ for the smaller streams and rivers, which falls on the high end of the range calculated for Q1 in the present study. The surface area of the river network is relatively evenly distributed amongst the four discharges classes of rivers (Table 2). Yet, river sections for which $Q < 10 \text{ m}^3 \text{ s}^{-1}$ (Q1+Q2) contribute to 65% of the total CO₂ outgassing although they only represent 51% of the surface area. This result therefore highlights that streams and small rivers are characterized by the highest surface-area specific emission rates. The higher outgassing rates in the North are a consequence of higher ΔCO_2 values since average k values are similar in both sections. In rivers with $Q_{\text{ann}} < 10 \text{ m}^3 \text{ s}^{-1}$, the ΔCO_2 is about twice as high in the North than in the South from April to August (Table 2). The calculation of pCO_2 from alkalinity and pH presumes however that all alkalinity originates from carbonate ions and thus tends to overestimate pCO_2 because non-carbonate contributions to alkalinity, in particular organic acids, are ignored in this approach. The rivers in Maine and New Brunswick, which drain most of the Northern part of COSCAT 827, are characterized by relatively low mineralized, low pH waters rich in organic matter. In these rivers, the overestimation in pCO_2 calculated from the carbonate alkalinity only was reported to be in the range 13%-66% (Hunt

et al., 2011). Considering that rivers in the Southern Part of COSCAT827 have lower DOC concentrations and higher DIC concentration, the higher FCO₂ rates per surface water area reported in the Northern part could partly be due to an overestimation of their pCO₂ values. However, a direct comparison of average pCO₂'s does not confirm this hypothesis. For the two Maine rivers (Kennebec and Androscoggin Rivers), Hunt et al. (2014) report an average pCO₂ calculated from pH and DIC of 3064 µatm. In our data set, three sampling stations are also located in these rivers and present lower median pCO₂ values of 2409, 901 and 1703 µatm for Kennebec River at Bingham and North Sidney and for Androscoggin River at Brunswick, respectively. A probable reason for the discrepancy could be that we report median values per month while Hunt et al. (2014) report arithmetic means, which are typically higher.

On the continental shelf, the shallowest depth interval is a CO₂ source in the North Section while all other depth intervals are CO₂ sinks (Table 2). The magnitude of the air-sea exchange for each segment is comprised between the values calculated for estuaries (50 gC m⁻² yr⁻¹) and the nearby open ocean (~20 gC m⁻² yr⁻¹, according to Takahashi et al., 2009). This trend along a depth transect, suggesting a more pronounced continental influence on near-shore waters and a strengthening of the CO₂ shelf sink away from the coast was already discussed in the regional analysis of Chavez et al. (2007) and by Jiang et al., (2013) specifically for the South Atlantic Bight. Modeling studies over a larger domain including the upper slope of the continental shelf also suggest that the coastal waters of the Northeast US are not a more intense CO₂ sink than the neighboring open ocean (Fennel and Wilkin, 2009; Fennel, 2010). Our analysis further suggests that the continental influence is more pronounced in the North section. Here, the shallowest waters (S1) are strong net sources of CO₂ while the intensity of the CO₂ sink for the other depth intervals gradually decreases, but only to a

maximum value of $-4 \text{ gC m}^{-2} \text{ yr}^{-1}$ for S5. This value is about 3 times smaller than in the South section ($-12 \text{ gC m}^{-2} \text{ yr}^{-1}$).

Annually, river and estuarine waters of the entire COSCAT 827 outgas $3.0 \pm 0.5 \text{ TgC yr}^{-1}$ and $0.8 \pm 0.5 \text{ TgC yr}^{-1}$, respectively, while continental shelf waters take up $1.7 \pm 0.3 \text{ TgC yr}^{-1}$ (Fig. 3c). The total riverine carbon load exported from rivers to estuaries for the same area has been estimated to 4.65 TgC yr^{-1} , 45% as dissolved and particulate organic carbon (2.10 TgC yr^{-1} , Mayorga et al., 2010) and 55% as dissolved inorganic carbon (2.55 TgC yr^{-1} , Hartmann et al., 2009). The ratio of organic to inorganic carbon in the river loads is about 1 in the North and 1.4 in the South. This difference stems mainly from a combination of different lithogenic characteristics in both sections and the comparatively higher occurrence of organic soils in the North (Hunt et al., 2013; Hossler and Bauer, 2013). Estimates of the total amount of terrestrial carbon transferred to the riverine network are not available but the sum of the river export and the outgassing, which ignores the contribution of carbon burial and lateral exchange with wetlands, provides a lower bound estimate of 7.65 TgC yr^{-1} . Under this hypothesis, ~40% of the terrestrial carbon exported to rivers is emitted to the atmosphere before reaching estuaries. In spite of higher emission rates per unit surface area in the North (Table 2), the overall efficiency of the riverine carbon filter is essentially the same in the two sections (40% and 38% outgassing for the North and the South, respectively). On the shelf, however, the South section exhibit a significantly more intense CO_2 sink ($-1.25 \pm 0.2 \text{ TgC yr}^{-1}$) than in the North ($-0.47 \pm 0.2 \text{ TgC yr}^{-1}$). A possible reason for this difference can be found in the contribution of the estuarine carbon filter. In the South, where 96% of the estuarine surface area is located, these systems contribute to an outgassing of 0.73 TgC yr^{-1} while in the North, their influence is negligible. Cole and Caraco (2001) estimated that 28% of the DOC entering the relatively short Hudson River estuary is respired in-situ before reaching the continental shelf and it is thus likely that the estuarine outgassing in the South section is

fueled by the respiration of the organic carbon loads from rivers. In contrast, the absence of estuaries in the North favors the direct export of terrestrial organic carbon onto continental shelf waters where it can be buried and decomposed. The respiration of terrestrial organic carbon could therefore explain why the strength of the shelf CO₂ sink is weaker in this portion of the domain. This view is further substantiated by the similar cumulated estuarine and continental shelf FCO₂ fluxes in both sections (Fig. 3a and b). Naturally, other environmental and physical factors also influence the carbon dynamics in shelf waters and contribute to the difference in CO₂ uptake intensity between both sections. For instance, in the North, the Gulf of Maine is a semi-enclosed basin characterized by specific hydrological features and circulation patterns (Salisbury et al., 2008; Wang et al., 2013) which could result in longer water residence times promoting the degradation of shelf-derived organic carbon. Other potential factors include the plume of the Saint Lawrence estuary, which has also been shown to transiently expend over the Scotian Shelf (Kang et al., 2013), the strong temperature gradient and the heterogeneous nutrient availability along the region which may result in different phytoplankton responses (Vandemark et al., 2011; Shadwick et al., 2011). Additionally, modeling studies evidenced the potential influence of sediment denitrification on water pCO₂ through the removal of fixed nitrogen in the water column and consequent inhibition of primary production (Fennel et al., 2008; Fennel, 2010). This removal was estimated to be of similar magnitude as the lateral nitrogen loads, except for estuaries of the MAB region (Fennel, 2010). It can nonetheless be suggested that the estuarine carbon filter in the South section of COSCAT 827 is an important control factor of the CO₂ sink in the Mid-Atlantic Bight, which is stronger than in any other area along the entire Atlantic coast of the US (Signorini et al., 2013).

381

382 **4. Conclusions**

383 Our data driven spatially and seasonally resolved budget analysis captures the main
384 characteristics of the air-water CO₂ exchange along the LOAC of COSCAT 827. It evidences
385 the contrasting dynamics of the North and South section of the study area and an overall
386 gradual shift from a strong source in small streams oversaturated in CO₂ towards a net sink in
387 continental shelf waters. Our study reveals that ice and snow cover are important controlling
388 factors of the seasonal dynamics of CO₂ outgassing in streams and rivers and account for a
389 large part of the difference between the North and South section. The close simultaneity of the
390 snow melts on land and of the phytoplankton bloom on the continental shelf leads to opposite
391 temporal dynamics in FCO₂ in these two compartments of the LOAC. In addition, our results
392 reveal that estuaries filter significant amounts of terrestrial carbon inputs, thereby influencing
393 the continental shelf carbon uptake. Although this process likely operates in conjunction with
394 other regional physical processes, it is proposed that the much stronger estuarine carbon filter
395 in the South section contributes to a strengthening of the CO₂ sink in the adjacent continental
396 shelf waters.

397

398 **Acknowledgements**

399 The research leading to these results has received funding from the European Union's
400 Seventh Framework Program (FP7/2007-2013) under grant agreement no. 283080, project
401 GEOCARBON. Goulven G. Laruelle is 'Chargé de recherches du F.R.S.-FNRS' at the
402 Université Libre de Bruxelles. Ronny Lauerwald was funded by the French Agence Nationale
403 de la Recherche (n° ANR-10-LABX-0018). Jens Hartmann was funded by DFG-project EXC
404 177. The Surface Ocean CO₂ Atlas (SOCAT) is an international effort, supported by the

405 International Ocean Carbon Coordination Project (IOCCP), the Surface Ocean Lower
406 Atmosphere Study (SOLAS), and the Integrated Marine Biogeochemistry and Ecosystem
407 Research program (IMBER), to deliver a uniformly quality-controlled surface ocean CO₂
408 database. The many researchers and funding agencies responsible for the collection of data
409 and quality control are thanked for their contributions to SOCAT. This work also used data
410 extracted from the SOCAT/MARCATS segmentation (Laruelle et al., 2013), the CCMP wind
411 database (Atlas et al., 2010), GLOBALNEWS2 (Mayorga et al., 2010; Hartmann et al., 2009),
412 the SRTM water body data set (NASA/NGA, 2003), Hydrosheds 15s routing scheme, the
413 average annual runoff data extracted from the UNH/GRDC composites (Fekete et al., 2002),
414 the global lake and wetland data base of Lehner and Döll (2004) and mean air temperature
415 derived from the worldclim data set of Hijmans et al. (2005).

416

References

- Aufdenkampe, A. K., Mayorga, E., Raymond, P. A., Melack, J. M., Doney, S. C., Alin, S. R., Aalto, R. E., and Yoo, K.: Riverine coupling of biogeochemical cycles between land, oceans, and atmosphere, *Frontiers in Ecology and the Environment*, 9(1), 53-60, doi:10.1890/100014, 2011.
- Armstrong, R. L., and Brodzik, M. J.: Recent Northern Hemisphere snow extent: A comparison of data derived from visible and microwave satellite sensors, *Geophysical Research Letters*, 28(19), 3673-3676, 2001.
- Atlas, R., Hoffman, R. N., Ardizzone, J., Leidner, S. M., Jusem, J. C., Smith, D. K., and Gombos, D.: A cross-calibrated, multiplatform ocean surface wind velocity product for meteorological and oceanographic applications, *Bull. Amer. Meteor. Soc.*, 92, 157-174. doi: 10.1175/2010BAMS2946.1, 2011.
- Bakker, D. C. E., Pfeil, B., Smith, K., Hankin, S., Olsen, A., Alin, S. R., Cosca, C., Harasawa, S., Kozyr, A., Nojiri, Y., O'Brien, K. M., Schuster, U., Telszewski, M., Tilbrook, B., Wada, C., Akl, J., Barbero, L., Bates, N. R., Boutin, J., Bozec, Y., Cai, W.-J., Castle, R. D., Chavez, F. P., Chen, L., Chierici, M., Currie, K., de Baar, H. J. W., Evans, W., Feely, R. A., Fransson, A., Gao, Z., Hales, B., Hardman-Mountford, N. J., Hoppema, M., Huang, W.-J., Hunt, C. W., Huss, B., Ichikawa, T., Johannessen, T., Jones, E. M., Jones, S. D., Jutterström, S., Kitidis, V., Körtzinger, A., Landschützer, P., Lauvset, S. K., Lefèvre, N., Manke, A. B., Mathis, J. T., Merlivat, L., Metzl, N., Murata, A., Newberger, T., Omar, A. M., Ono, T., Park, G.-H., Paterson, K., Pierrot, D., Rios, A. F., Sabine, C. L., Saito, S., Salisbury, J., Sarma, V. V. S. S., Schlitzer, R., Sieger, R., Skjelvan, I., Steinhoff, T., Sullivan, K. F., Sun, H., Sutton, A. J., Suzuki, T., Sweeney, C., Takahashi, T., Tjiputra, J., Tsurushima, N., van Heuven, S. M. A. C., Vandemark, D., Vlahos, P., Wallace, D. W. R.,

441 Wanninkhof, R., and Watson, A. J.: An update to the Surface Ocean CO₂ Atlas (SOCAT
 442 version 2), *Earth Syst. Sci. Data*, 6, 69-90, doi:10.5194/essd-6-69-2014, 2014.

443 Battin, T. J., Luyssaert, S., and Kaplan, L. A.: The boundless carbon cycle, *Nat. Biogeosci.*, 2,
 444 598-600, 2009.

445 Bauer, J. E., Cai, W.-J., Raymond, P. A., Bianchi, T. S., Hopkinson, C. S., and Regnier, P. A.
 446 G.: The changing carbon cycle of the coastal ocean, *Nature*, 504, 61-70, doi:
 447 10.1038/nature12857, 2013.

448 Borges, A. V., Delille, B., and Frankignoulle, M.: Budgeting sinks and sources of CO₂ in the
 449 coastal ocean: diversity of ecosystems counts, *Geophysical Research Letters* 32, L14601.
 450 doi:10.1029/2005GL023053, 2005.

451 Butman, D., and Raymond, P. A.: Significant efflux of carbon dioxide from streams and
 452 rivers in the United States, *Nature Geoscience*, 4(12), 839–842, 2011.

453 Cai, W. J.: Estuarine and coastal ocean carbon paradox: CO₂ sinks or sites of terrestrial
 454 carbon incineration? *Annu. Rev. Mar. Sci.*, 3, 123-145, 2011.

455 Ciais, P., et al. (2013) Chapter 6: Carbon and Other Biogeochemical Cycles, in: *Climate*
 456 *Change 2013 The Physical Science Basis*. Cambridge University Press, Cambridge.
 457 Stocker, T., D. Qin, and G.-K. Plattner (eds.)

458 Chavez, F. P., Takahashi, T., Cai, W. -J., Friederich, G., Hales, B., Wanninkhof, R., and
 459 Feely, R.: Coastal oceans. The First State of the Carbon Cycle Report (SOCCR): The
 460 North American Carbon Budget and Implications for the Global Carbon Cycle: 157-166.
 461 King A. W., Dilling L., Zimmerman G. P., Fairman D. M., Houghton R. A., Marland G.,
 462 Rose A. Z., Wilbanks T. J. (eds.), 2007.

463 Chen, C. T. A., Huang, T. H., Chen, Y. C., Bai, Y., He, X., and Kang, Y.: Air-sea exchanges
 464 of CO₂ in the world's coastal seas, *Biogeosciences*, 10, 6509-6544, doi:10.5194/bg-10-
 465 6509-2013, 2013.

466 Cole, J. J., and Caraco, N. F.: Carbon in catchments: Connecting terrestrial carbon losses with
 467 aquatic metabolism, *Mar. Freshwater Res.*, 52(1), 101-110, doi:10.1071/MF00084, 2001.

468 Cole, J. J., Prairie, Y. T., Caraco, N. F., McDowell, W. H., Tranvik, L. J., Striegl, R. G.,
 469 Duarte, C. M., Kortelainen, P., Downing, J. A., Middelburg, J. J., and Melack, J.:
 470 Plumbing the global carbon cycle: Integrating inland waters into the terrestrial carbon
 471 budget, *Ecosystems*, 10, 171–184, 2007.

472 Dai, M., Cao, Z., Guo, X., Zhai, W., Liu, Z., Yin, Z., Xu, Y., Gan, J., Hu, J., and Du, C.:
 473 Why are some marginal seas sources of atmospheric CO₂? *Geophys. Res. Lett.*, 40, 2154-
 474 2158, 2013.

475 Degrandpré, M. D., Olbu, G. J., Beatty, M., and Hammar, T. R.: Air-sea CO₂ fluxes on the
 476 US Middle Atlantic Bight, *Deep-Sea Res. II*, 49, 4355-4367, 2002.

477 Fekete, B. M., Vorosmarty, C. J., Grabs, W., and Vörösmarty, C. J.: High-resolution fields of
 478 global runoff combining observed river discharge and simulated water balances, *Global*
 479 *Biogeochemical Cycles*, 16(3), doi 10.1029/1999gb001254, 2002.

480 Fennel, K.: The role of continental shelves in nitrogen and carbon cycling:Northwestern
 481 North Atlantic case study. *Ocean Science*, 6, 539-548, doi:10.5194/os-6-539-2010, 2010.

482 Fennel, K., and Wilkin, J.: Quantifying biological carbon export for the northwest North
 483 Atlantic continental shelves, *Geophysical Research Letters*, 36, L18605,
 484 doi:10.1029/2009GL039818, 2009.

485 Fennel, K., Wilkin, J., Previdi, M., and Najjar, R.: Denitrification effects on air-sea CO₂ flux
 486 in the coastal ocean: Simulations for the Northwest North Atlantic, *Geophysical Research*
 487 *Letters*, 35, L24608, doi:10.1029/2008GL036147, 2008.

488 Frankignoulle, M., Abril, G., Borges, A., Bourge, I., Canon, C., Delille, B., Libert, E., and
 489 Théate, J.-M.: Carbon dioxide emission from European estuaries, *Science*, 282, 434-436,
 490 doi:10.1126/science.282.5388.434, 1998.

491 Finlay, C. F.: Controls of streamwater dissolved inorganic carbon dynamics in a forested
 492 watershed, *Biogeochem.*, 62, 231-252, 2003.

493 Hartmann, J., Lauerwald, R., and Moosdorf, N.: A brief overview of the GLObal River
 494 CHemistry Database, GLORICH, *Procedia - Earth and Planetary Science*, 10, 23-27,
 495 2014.

496 Hartmann, J., Jansen, N., Dürr, H. H., Kempe, S., and Köhler, P.: Global CO₂-consumption
 497 by chemical weathering: What is the contribution of highly active weathering regions?,
 498 *Global and Planetary Change*, 69(4), 185-194, doi:10.1016/j.gloplacha.2009.07.007, 2009.

499 Henry, W.: Experiments on the Quantity of Gases Absorbed by Water, at Different
 500 Temperatures, and under Different Pressures, *Philosophical Transactions of the Royal*
 501 *Society*, 93, 29-274, doi:10.1098/rstl.1803.0004, 1803.

502 Hijmans, R. J., Cameron, S. E., Parra, J. L., Jones, P. G., and Jarvis, A.: Very high resolution
 503 interpolated climate surfaces for global land areas, *International Journal of Climatology*,
 504 25(15), 1965-1978, doi:10.1002/joc.1276, 2005.

505 Hossler, K., and Bauer, J. E.: Amounts, isotopic character, and ages of organic and inorganic
 506 carbon exported from rivers to ocean margins: 1. Estimates of terrestrial losses and inputs

507 to the Middle Atlantic Bight, *Global Biogeochemical Cycles*, 27(2), 331-346, doi:
508 10.1002/gbc.20033, 2013

509 Hunt, C. W., Salisbury, J. E., and Vandemark, D.: Contribution of non-carbonate anions to
510 total alkalinity and overestimation of pCO₂ in New England and New Brunswick rivers.
511 *Biogeosciences*, 8(10), 3069-3076, doi:10.5194/bg-8-3069-2011, 2011.

512 Hunt, C. W., Salisbury, J. E., and Vandemark, D.: CO₂ Input Dynamics and Air-Sea
513 Exchange in a Large New England Estuary. *Estuaries and Coasts*, 37(5), 1078–1091,
514 2014.

515 Hunt, C. W., Salisbury, J. E., Vandemark, D., and McGillis, W.: Contrasting Carbon Dioxide
516 Inputs and Exchange in Three Adjacent New England Estuaries. *Estuaries and Coasts*, 34,
517 68-77, doi: 10.1007/s12237-010-9299-9, 2010.

518 Jiang, L.-Q., Cai, W.-J., Wang, Y., and Bauer, J. E.: Influence of terrestrial inputs on
519 continental shelf carbon dioxide, *Biogeosciences*, 10, 839-849, doi:10.5194/bg-10-839-
520 2013, 2013.

521 Jones, J. B., and Mulholland, P. J.: Carbon dioxide variation in a hardwood forest stream: An
522 integrative measure of whole catchment soil respiration, *Ecosystems*, 1(2), 183-196, 1998.

523 Kang, Y., Pan, D., Bai, Y., He, X., Chen, X., Chen, C.-T. A., and Wang, D.: Areas of the
524 global major river plumes, *Acta Oceanol. Sin.*, 32(1), 1-10, doi: 10.1007/s13131-013-
525 0213-0, 2013.

526 Kempe, S.: Long-term records of CO₂, pressure fluctuations in fresh waters. *Mitt. Geol.-*
527 *Palaeontol. Inst. Univ. Hamburg* 52(1): 9, 1-332, 1982.

528 Laruelle, G. G., Dürr, H. H., Lauerwald, R., Hartmann, J., Slomp, C. P., Goossens, N., and
 529 Regnier, P. A. G.: Global multi-scale segmentation of continental and coastal waters from
 530 the watersheds to the continental margins, *Hydrol. Earth Syst. Sci.*, 17, 2029-2051,
 531 doi:10.5194/hess-17-2029-2013, 2013.

532 Laruelle, G. G., Dürr, H. H., Slomp, C. P., and Borges, A. V.: Evaluation of sinks and sources
 533 of CO₂ in the global coastal ocean using a spatially-explicit typology of estuaries and
 534 continental shelves, *Geophys. Res. Lett.*, 37, L15607, doi:10.1029/2010GL043691, 2010.

535 Laruelle, G. G., Lauerwald, R., Pfeil, B., and Regnier P.: Regionalized global budget of the
 536 CO₂ exchange at the air-water interface in continental shelf seas, *Global Biogeochemical*
 537 *Cycles*, 28, doi: 10.1002/2014GB004832, 2014.

538 Lauerwald, R., Hartmann, J., Moosdorf, N., Kempe, S., and Raymond, P. A.: What controls
 539 the spatial patterns of the riverine carbonate system? - A case study for North America.,
 540 *Chemical Geology*, 337-338, 114-127, 2013.

541 Lauerwald, R., Laruelle, G. G., Hartmann, J., Ciais, P., Regnier, P. A. G.: Spatial patterns in
 542 CO₂ evasion from the global river network *Global Biogeochemical Cycles*, under
 543 revisions.

544 Lehner, B., and Döll, P.: Development and validation of a global database of lakes, reservoirs
 545 and wetlands, *Journal of Hydrology*, 296(1-4), 1-22, doi: 10.1016/j.jhydrol.2004.03.028,
 546 2004.

547 Lehner, B., Verdin, K., and Jarvis, A.: New global hydrography derived from spaceborne
 548 elevation data, *Eos, Transactions, AGU*, 89(10), 93-94, 2008.

549 Mackenzie, F. T., De Carlo, E. H., and Lerman, A.: Coupled C, N, P, and O Biogeochemical
550 Cycling at the Land-Ocean Interface. In: Middelburg J. J., Laane R. (eds.) Treatise on
551 Estuarine and Coastal Science. Elsevier, 2012.

552 Mayorga, E., Seitzinger, S. P., Harrison, J. A., Dumont, E., Beusen, A. H. W., Bouwman, A.
553 F., Fekete, B. M., Kroeze, C., and Van Drecht, G.: Global Nutrient Export from
554 WaterSheds 2 (NEWS2): Model development and implementation, Environ. Model.
555 Softw., 25, 837-853, doi:10.1016/j.envsoft.2010.01.007, 2010.

556 Meybeck, M., Dürr, H. H., and Vörosmary, C. J.: Global coastal segmentation and its river
557 catchment contributors: A new look at land-ocean linkage. Global Biogeochemical
558 Cycles, 20, GB1S90:1-15, doi: 10.1029/2005GB002540, 2006.

559 NASA/NGA: SRTM Water Body Data Product Specific Guidance, Version 2.0, 2003.

560 Parkhurst, D. L., and Appelo, C. A. J.: User's guide to PHREEQC (version 2) - a computer
561 program for speciation, reaction-path, 1D-transport, and inverse geochemical calculations,
562 US Geol. Surv. Water Resour. Inv. Rep., 99-4259, 1999.

563 Previdi, M., Fennel, K., Wilkin, J., and Haidvogel, D.B.: Interannual Variability in
564 Atmospheric CO₂ Uptake on the Northeast U.S. Continental Shelf, Journal of Geophysical
565 Research, 114, G04003, doi:10.1029/2008JG000881, 2009.

566 Raymond, P. A., and Hopkinson, C. S.: Ecosystem Modulation of Dissolved Carbon Age in a
567 Temperate Marsh-Dominated Estuary, Ecosystems, 6(7), 694-705, 2003.

568 Raymond, P. A., Bauer, J. E., and Cole, J. J.: Atmospheric CO₂ evasion, dissolved inorganic
569 carbon production, and net heterotrophy in the York River estuary. Limnol. Oceanogr.,
570 45(8), 1707-1717, 2000.

571 Raymond, P. A., Caraco, N. F., and Cole, J. J.: Carbon Dioxide Concentration and
572 Atmospheric Flux in the Hudson River, *Estuaries*, 20(2), 381-390, 1997.

573 Raymond, P. A., Zappa, C. J., Butman, D., Bott, T. L., Potter, J., Mulholland, P., Laursen, A.
574 E., McDowell, W. H., and Newbold, D.: Scaling the gas transfer velocity and hydraulic
575 geometry in streams and small rivers, *Limnology & Oceanography: Fluids &
576 Environments*, 2, 41-53, doi:10.1215/21573689-1597669, 2012.

577 Raymond, P. A., Hartmann, J., Lauerwald, R., Sobek, S., McDonald, C., Hoover, M.,
578 Butman, D., Striegl, R., Mayorga, E., Humborg, C., Kortelainen, P., Dürr, H., Meybeck,
579 M., Ciais, P., and Guth, P.: Global carbon dioxide emissions from inland waters, *Nature*,
580 503(7476), 355-359, doi: 10.1038/nature12760, 2013.

581 Rawlins, B. G., Palumbo-Roe, B., Gooddy, D. C., Worrall, F., and Smith, H.: A model of
582 potential carbon dioxide efflux from surface water across England and Wales using
583 headwater stream survey data and landscape predictors, *Biogeosciences*, 11(7), 1911-
584 1925, 2014.

585 Regnier, P., Friedlingstein, P., Ciais, P., Mackenzie, F. T., Gruber, N., Janssens, I., Laruelle,
586 G. G., Lauerwald, R., Luyssaert, S., Andersson, A. J., Arndt, S., Arnosti, C., Borges, A.
587 V., Dale, A. W., Gallego-Sala, A., Godd  ris, Y., Goossens, N., Hartmann, J., Heinze, C.,
588 Ilyina, T., Joos, F., LaRowe, D. E., Leifeld, J., Meysman, F. J. R., Munhoven, G.,
589 Raymond, P. A., Spahni, R., Suntharalingam, P., and Thullner, M.: Anthropogenic
590 perturbation of the carbon fluxes from land to ocean. *Nature Geoscience*, 6(8), 597-607,
591 doi:10.1038/ngeo1830, 2013.

592 Salisbury, J. E., Vandemark, D., Hunt, C. W., Campbell, J. W., McGillis, W. R., and
593 McDowell, W. H.: Seasonal observations of surface waters in two Gulf of Maine estuary-

594 plume systems: Relationships between watershed attributes, optical measurements and
595 surface pCO₂, *Estuarine Coastal Shelf Sci.*, 77(2), 245-252, 2008.

596 Shadwick, E. H., Thomas, H., Azetsu-Scott, K., Greenan, B. J. W., Head, E., and Horne, E.:
597 Seasonal variability of dissolved inorganic carbon and surface water pCO₂ in the Scotian
598 Shelf region of the Northwestern, Atlantic, *Mar. Chem.*, 124(1-4), 23-37, 2011.

599 Shadwick, E. H., Thomas, H., Comeau, A., Craig, S. E., Hunt, C. W., and Salisbury, J. E.:
600 Air-Sea CO₂ fluxes on the Scotian Shelf: seasonal to multi-annual variability,
601 *Biogeosciences*, 7, 3851-3867, 2010.

602 Signorini, S. R., Mannino, A., Najjar Jr., R. G., Friedrichs, M. A. M., Cai, W.-J., Salisbury, J.,
603 Wang, Z. A., Thomas, H., and Shadwick, E.: Surface ocean pCO₂ seasonality and sea-air
604 CO₂ flux estimates for the North American east coast, *J. Geophys. Res. Oceans*, 118,
605 5439-5460, doi:10.1002/jgrc.20369, 2013.

606 Strahler, A. N.: Hypsometric (area-altitude) analysis of erosional topology, *Geological*
607 *Society of America Bulletin*, 63(11), 1117-1142, doi:10.1130/0016-7606, 1952.

608 Striegl, R. G., Dornblaser, M. M., McDonald, C. P., Rover, J. R., and Stets, E. G.: Carbon
609 dioxide and methane emissions from the Yukon River system, *Global Biogeochemical*
610 *Cycles*, 26(4), 2012.

611 Takahashi, T., Sutherland, S. C., Wanninkhof, R., Sweeney, C., Feely, R. A., Chipman, D.
612 W., Hales, B., Friederich, G., Chavez, F., Sabine, C., Watson, A., Bakker, D. C. E.,
613 Schuster, U., Metzl, N., Yoshikawa-Inoue, H., Ishii, M., Midorikawa, T., Nojiri, Y.,
614 Körtzinger, A., Steinhoff, T., Hoppema, M., Olafsson, J., Arnarson, T. S., Tilbrook, B.,
615 Johannessen, T., Olsen, A., Bellerby, R., Wong, C. S., Delille, B., Bates, N. R., and de

616 Baar, H. J. W.: Climatological mean and decadal change in surface ocean pCO₂, and net
617 sea-air CO₂ flux over the global oceans, *Deep-Sea Res. Pt. II*, 56, 554–577, 2009.

618 Telmer, K., and Veizer, J.: Carbon fluxes, pCO₂ and substrate weathering in a large northern
619 river basin, Canada: Carbon isotope perspectives, *Chem Geol*, 151, 61-86, 1999.

620 Teodoru, C. R., del Giorgio, P. A., Prairie, Y. T., and Camire, M.: Patterns in pCO₂ in boreal
621 streams and rivers of northern Quebec, Canada, *Global Biogeochemical Cycles*, 23(2),
622 GB2012, doi: 10.1029/2008GB003404, 2009.

623 Thomas, H., and Schneider, B.: The seasonal cycle of carbon dioxide in Baltic Sea surface
624 waters, *J. Mar. Syst.*, 22(1), 53-67, doi: 10.1016/s0924-7963(99)00030-5, 1999.

625 Vandemark, D, Salisbury, J. E, Hunt, C.W, Shellito, S. M, Irish, J. D, McGillis, W. R, Sabine,
626 C. L, and Maenner, S. M.: Temporal and spatial dynamics of CO₂ air-sea flux in the Gulf
627 of Maine. *Journal of Geophysical Research: Oceans*, 116(C1), C01012. doi:
628 10.1029/2010JC006408, 2011.

629 Wallin, M. B., Oquist, M. G., Buffam, I., Billett, M. F., Nisell, J., Bishop, K. H., and Öquist,
630 M. G.: Spatiotemporal variability of the gas transfer coefficient (K-CO₂) in boreal
631 streams: Implications for large scale estimates of CO₂ evasion, *Global Biogeochem.*
632 *Cycles*, 25(3), GB3025, doi:10.1029/2010gb003975, 2011.

633 Wang, Z. A., Wanninkhof, R., Cai, W.-J., Byrne, R. H., Hu, X., Peng, T. H., and Huang, W.
634 J.: The marine inorganic carbon system along the Gulf of Mexico and Atlantic Coasts of
635 the United States: Insights from a transregional coastal carbon study, *Limnol. Oceanogr.*,
636 58, 325-342, 2013.

637 Wanninkhof, R.: Relationship between wind speed and gas exchange over the ocean, *J.*
638 *Geophys. Res.*, 97, 7373-7382, 1992.

639 Wanninkhof, R., Park, G.-H., Takahashi, T., Sweeney, C., Feely, R., Nojiri, Y., Gruber, N.,
640 Doney, S. C., McKinley, G. A., Lenton, A., Le Quéré, C., Heinze, C., Schwinger, J.,
641 Graven, H., and Khatiwala, S.: Global ocean carbon uptake: magnitude, variability and
642 trends, *Biogeosciences*, 10, 1983–2000, doi:10.5194/bg-10-1983-2013, 2013.

643

644 **Figure captions:**

645 Figure 1: Geographic limits of the study area with the location of the riverine (Glorich
646 database, in green; Lauerwald et al., 2013) and continental shelf waters data used for our
647 calculations (SOCAT 2.0 database, in red; Bakker et al., 2014). The location of the estuarine
648 studies used is indicated by purple squares.

649 Figure 2: Spatial distribution of the CO₂ exchange with the atmosphere in rivers and
650 continental shelf waters aggregated by seasons. The fluxes are net FCO₂ rates averaged over
651 the surface area of each 0.25° cells and a period of 3 months. Positive values correspond to
652 fluxes towards the atmosphere. Winter is defined as January, February and March, Spring as
653 April, May and June and so forth.

654 Figure 3: Areal-integrated monthly air-water CO₂ flux for rivers and the continental shelf
655 waters in the North section (a), South section (b), and entire study area (c). Positive values
656 correspond to fluxes towards the atmosphere. The boxes inside each panel correspond to the
657 annual carbon budgets for the region including the lateral carbon fluxes at the river-estuary
658 interface, as inorganic (IC) and organic carbon (OC). The values in grey represent the
659 uncertainties of the annual fluxes.

660

661 **Table 1:** Summary of the data used for the FCO₂ calculations in compartment of the LOAC.

Compartment	Parameter	Description	Source	Reference
Rivers	pCO_2	CO ₂ partial pressure	GLORICH	Hartmann et al., 2014; Lauerwald et al., 2013 Lehner et al., 2008
	-	River network, digital elevation model (DEM)	Hydrosheds 15s	
	-	Runoff	UNH/GRDC	Fekete et al., 2002
Estuaries	T	Air-temperature	-	Hijmans et al., 2005
	As	Lake surface area	Global Lake and Wetland Database	Lehner and Döll, 2004
	As	Surface Area	SRTM water body data set	NASA/NGA, 2003
	-	CO ₂ exchange rate	Average of local estimates	Raymond et al., 1997; Raymond et al., 2000; Raymond and Hopkinson, 2003; Hunt et al., 2010
Shelves	As	Surface area	COSCAT/MARCATS Segmentation	Laruelle et al., 2013
	ΔpCO_2	pCO ₂ gradient at the air-water interface	SOCAT database	Bakker et al., 2014
	k	calculated using wind Speed	CCMP database	Altas et al., 2011
	K'_0	Solubility, calculated using salinity, water temperature	SOCAT database	Bakker et al., 2014

662

663

664

665 **Table 2:** Surface areas, CO₂ exchange rate with the atmosphere and surface integrated FCO₂ for the North and South sections of COSCAT 827,
 666 subdivided by river discharge classes and continental shelf water depth intervals.

	North			South			Total		
	Surface Area	Rate	FCO ₂	Surface Area	Rate	FCO ₂	Surface Area	Rate	FCO ₂
	10 ³ km ²	gCm ⁻² yr ⁻¹	10 ⁹ gC yr ⁻¹	10 ³ km ²	gCm ⁻² yr ⁻¹	10 ⁹ gC yr ⁻¹	10 ³ km ²	gCm ⁻² yr ⁻¹	10 ⁹ gC yr ⁻¹
Rivers									
Q1 (Q < 1m s⁻¹)	0.14	2893±521	391±70	0.27	1961±353	532±96	0.41	2271±409	924±166
Q2 (1m s⁻¹ < Q < 10m s⁻¹)	0.21	2538±457	525±95	0.32	1570±283	506±91	0.53	1948±351	1032±186
Q3 (10m s⁻¹ < Q < 100m s⁻¹)	0.16	1476±267	237±43	0.30	1307±235	392±71	0.46	1366±246	629±113
Q4 (100m s⁻¹ < Q)	0.17	891±160	152±27	0.36	729±131	261±47	0.52	781±141	412±74
Sub-total	0.67	1939±349	1305±235	1.25	1351±243	1692±305	1.92	1557±280	2997±539
Estuaries	0.53	50 ± 31	27 ± 19	14.51	50 ± 31	731 ± 453	15.04	50 ± 31	758 ± 469
Shelf									
S1 (depth < 20m)	11.21	5 ± 1	53 ± 19	24.28	-3 ± 1	-79 ± 11	35.49	-1 ± 1	-27 ± 5
S2 (20m < depth < 50m)	26.25	-1 ± 1	-35 ± 12	63.88	-8 ± 1	-521 ± 70	90.13	-6 ± 1	-556 ± 108
S3 (50m < depth < 80m)	39.28	-3 ± 1	-128 ± 45	48.63	-7 ± 1	-359 ± 126	87.91	-6 ± 1	-488 ± 95
S4 (80m < depth < 120m)	60.69	-3 ± 1	-209 ± 73	25.18	-8 ± 1	-199 ± 27	85.87	-5 ± 1	-409 ± 80
S5 (120m < depth < 150m)	34.73	-4 ± 1	-151 ± 18	7.63	-12 ± 1	-91 ± 12	42.36	-6 ± 1	-242 ± 47
Sub-total	172.17	-3 ± 1	-472±166	169.59	-7 ± 1	-1250±169	341.77	-5 ± 1	-1722±335

667

668

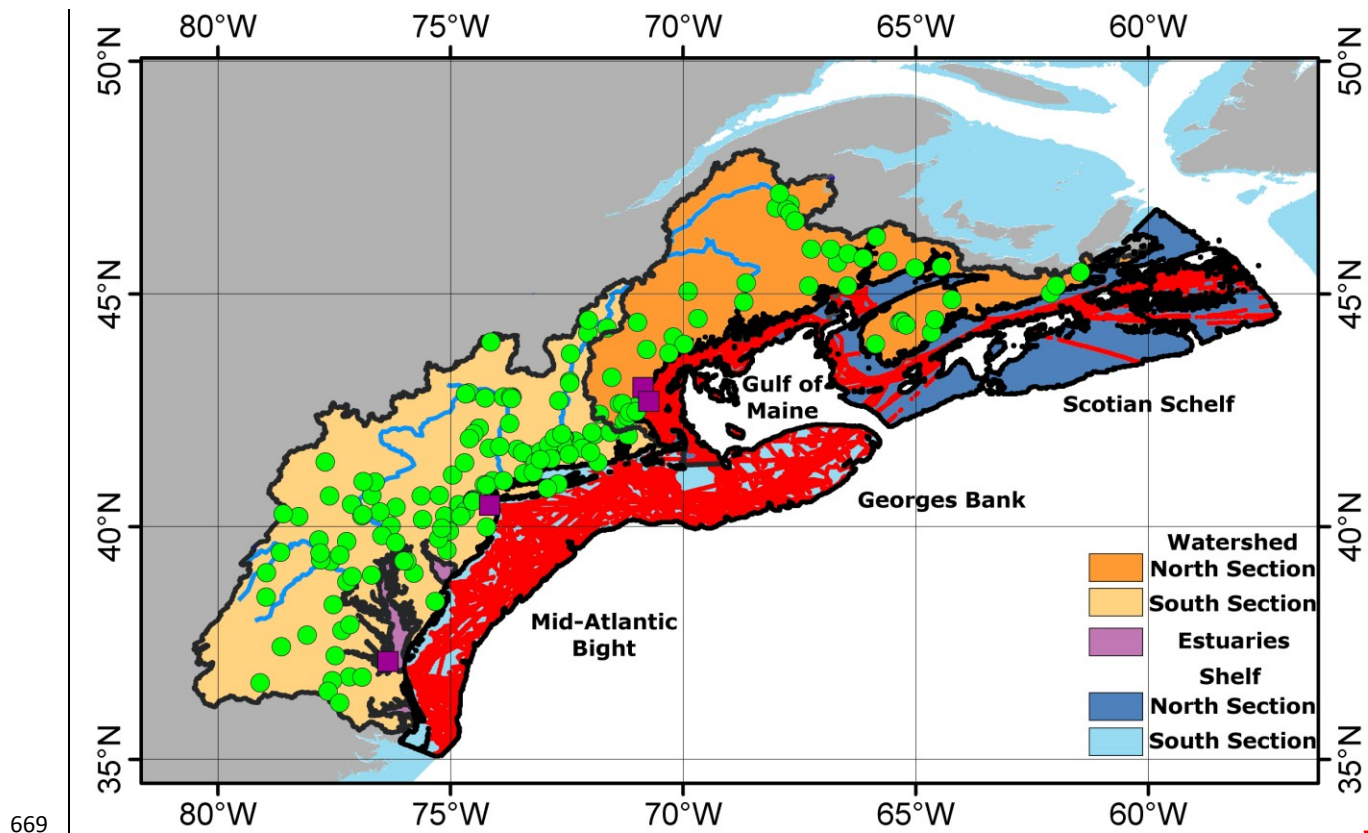
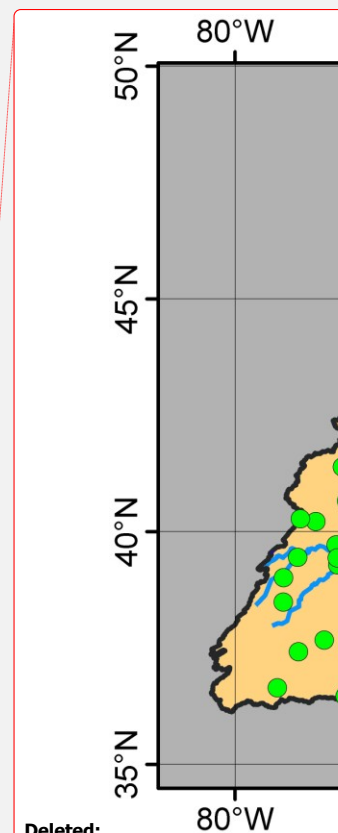


Figure 1 (updated)



Deleted:

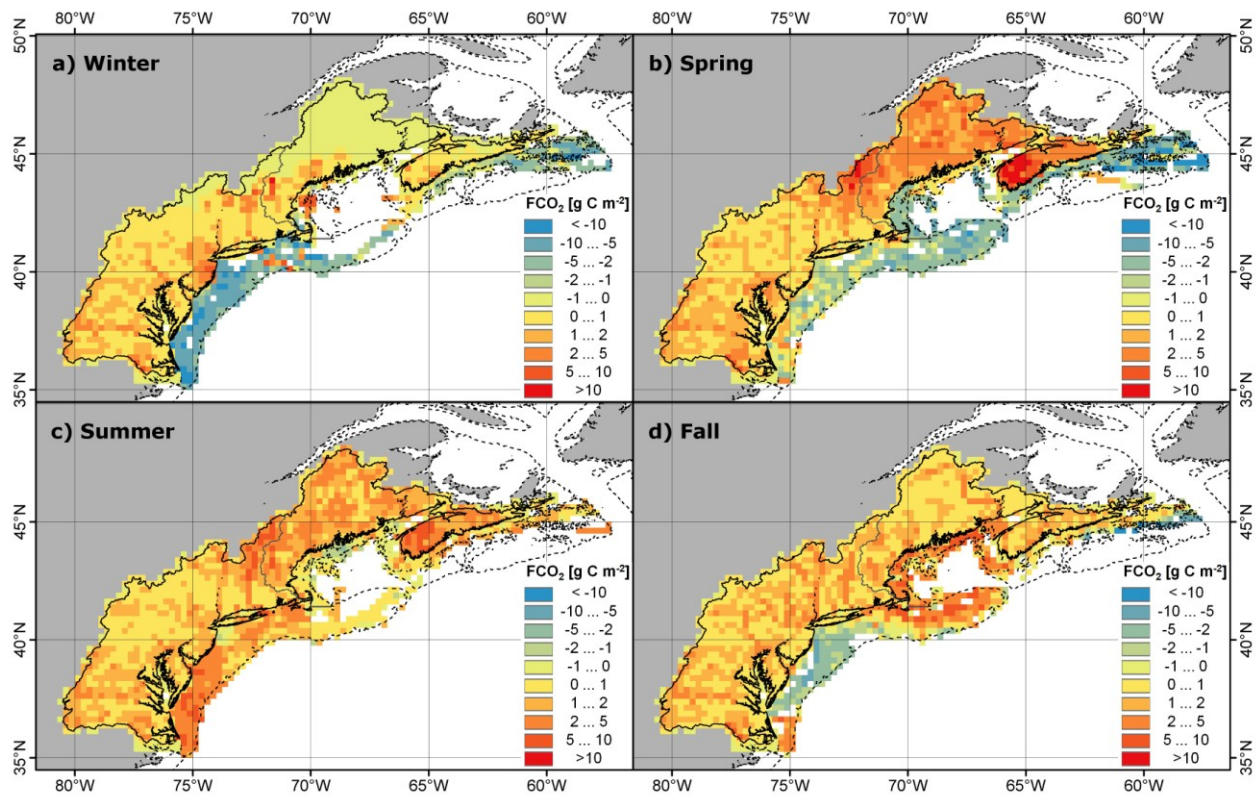
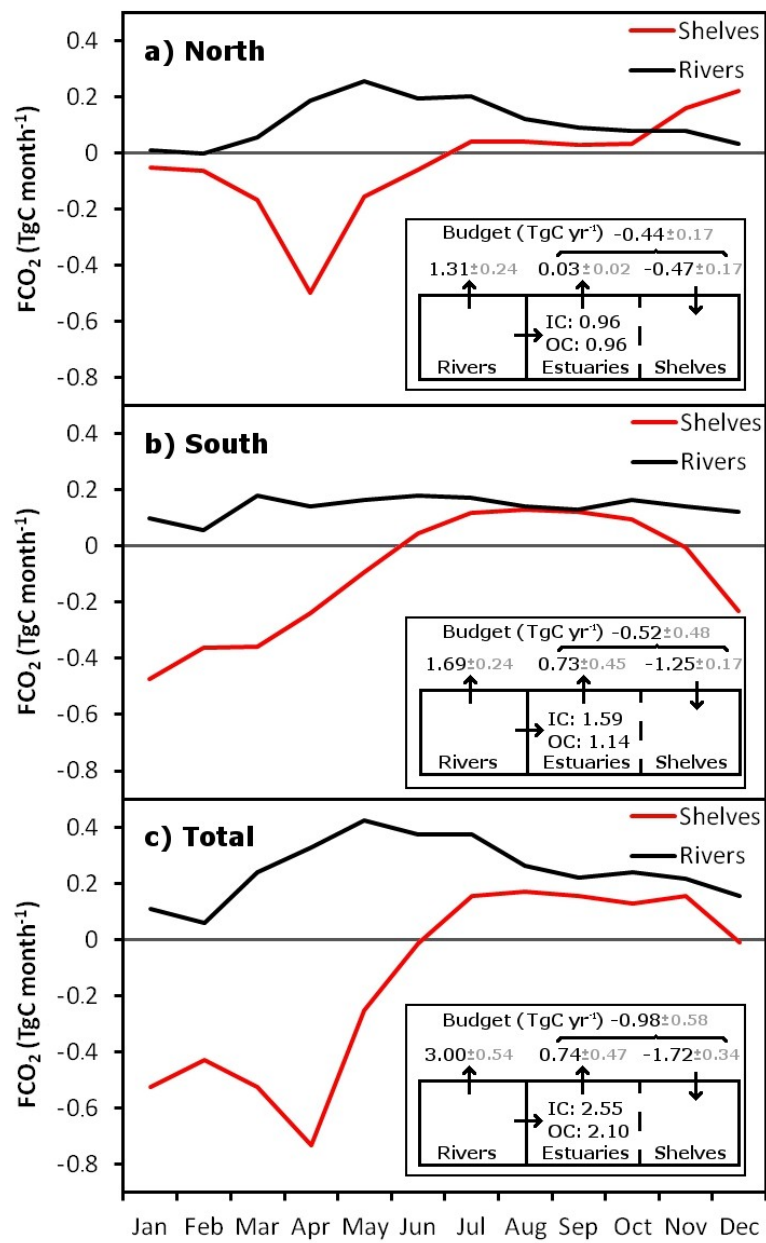


Figure 2



676

677 **Figure 3**